www.czasopisma.pan.pl PAN www.journals.pan.pl

ARCHIVES of FOUNDRY ENGINEERING

ISSN (2299-2944)
Volume 2020
Issue 2/2020

26 – 30

4/2

10.24425/afe.2020.131297

Published quarterly as the organ of the Foundry Commission of the Polish Academy of Sciences

Electrochemical Corrosion Evaluation of Copper-Alloyed Ductile Cast Irons

P. Brito *, W. Pereira, W. Santos, H. Gomes
Pontifical Catholic University of Minas Gerais, Brazil
* Corresponding author. E-mail address: pbrito@pucminas.br

Received 08.08.2019; accepted in revised form 15.01.2020

Abstract

In the present work, different Cu-alloyed model ductile irons with ferritic (0%Cu-0.09%Mn), mixed ferritic-pearlitic (0.38%Cu-0.40%Mn) and pearlitic (0.69%Cu-0.63%Mn) microstructure were produced and analyzed in terms of their electrochemical corrosion behavior in a 3.5wt.%NaCl aqueous solution containing naturally dissolved oxygen at room temperature (25°C). The remaining elements such as Si and Mg were kept at balanced levels in an attempt to minimize variations in graphite size and distribution among different samples. The corrosion resistance was evaluated by electrochemical impedance spectroscopy and potentiodynamic polarization. Microstructure analysis of the cast alloys confirmed similarity in the graphite morphology among the different cast samples and the expected variations in the metallic matrix. In the absence of passivation, it was found that the addition of copper led to an increase in corrosion resistance, which could be attested by higher values polarization resistance and corrosion potential.

Keywords: Environment protection, Metallography, Ductile Iron, Corrosion, Copper

1. Introduction

Ductile cast irons have many important characteristics as engineering materials such as low cost, machinability, mechanical strength and wear resistance. The main microstructural features which affect the mechanical properties of ductile cast irons are distribution, geometry and size of graphite nodules, size and morphology of primary dendrites, ferrite/pearlite ratio, ferritic grain size and pearlite interlamellar spacing [1]. Currently, ductile cast iron castings are employed in relevant applications which involve corrosion in chloride containing media (*e.g.* coastal of offshore locations), such as windmill wheel, chassis and rotor housings [2, 3], sea water pumps and valves used in petrochemical plants and refineries [4], buried pipelines [5], among others.

With the expansion of the use of ductile iron castings, the interest in the electrochemical corrosion resistance of these alloys has increased. So far, attempts to improve corrosion behavior of ductile cast irons have been pursued either by the application of surface modification techniques [6] or by adjusting chemical composition, with or without heat treatment [7-11]. The latter approach, involving composition and/or microstructure is considered promising to produce large or complex shaped castings.

Based on these considerations, in the present work an experimental investigation was carried out in order to evaluate the influence of ductile cast iron composition and microstructure on the electrochemical corrosion behavior.

2. Experimental procedure

In the present work, ductile cast irons of three compositions were selected in order to produce variations in the metal alloy matrix: ferritic (F), ferritic-pearlitic (FP) and pearlitic (P). In each case, standard Y-block castings (following ASTM A536) were produced in an induction furnace with 50 kg load. The chemical composition of the alloys was analyzed by optical emission

spectroscopy (Table 1). In order to obtain a completely ferritic matrix in sample F, the castings were subject to annealing at 900°C and slowly cooled to room temperature. The remaining samples were analyzed in the as-cast condition.

The chemical composition was adjusted in order to allow variations in the matrix without changes in graphite nodule morphology and quantity. In this sense, the levels of Mn and Cu, which favor the formation of pearlite were varied, while C, Si and Mg, associated with the inoculation and nodularization process remained constant [12]. In the present work, it was considered important to maintain even graphite nodule characteristics since the sharp difference in reduction potential between graphite and iron could produce galvanic effects with the metallic matrix and influence corrosion behavior.

Table 1.
Chemical composition of the alloys used in the present work, according to matrix: ferritic (F), ferritic-pearlitic (FP) and pearlitic (P). Values in weight %.

Sample	C	Si	Mn	P	S	Cr	Cu	Mg
F	3.81	2.57	0.09	0.10	0.007	0.03	-	0.034
FP	3.66	2.52	0.40	0.08	0.009	0.02	0.38	0.034
P	3.71	2.39	0.63	0.10	0.008	0.02	0.69	0.031

Samples for microstructure analysis were cut from the cast blocks and prepared following standard metallographic procedure. The characterization of graphite nodules was performed according to ASTM A247 and ASTM E2567 standards with assistance of the ImageJ software. The minimum nodule size considered for evaluation was 10 µm and a minimum shape factor (circularity) was 0.6. The samples used for graphite nodule analysis were not etched, while samples for microstructure analysis were etched in a Nital 2% solution. The hardness of the cast materials was evaluated by the Brinell method, using a 2.5 mm indenter with a 62.5 kgf load. A total of 20 measurements was performed on each alloy.

The electrochemical corrosion behavior of all three castings was evaluated. The tests were performed in a NaCl solution (3.5wt.%) in the aerated condition (containing naturally dissolved oxygen). The equipment used in the corrosion analyses was an IVIUM Vertex potentiostat galvanostat connected to a 500 ml electrochemical cell for flat specimens containing a 10 mm diameter circular orifice for exposing the samples to the electrolyte. The cell was mounted with a three-electrode configuration: working electrode (sample), Pt-wire counter electrode and Ag/AgCl (in saturated KCl) reference electrode.

The open-circuit potential (OCP) was monitored for 1.5 h. At the stabilized OCP, electrochemical impedance spectroscopy (EIS) analyses were conducted within a frequency range of 100,000 to 0.01 Hz, 10 mV sinusoidal excitation signal and data acquisition rate of 10 points per decade. Equivalent circuit models were employed to analyze the EIS data, by using IviumSoft software version 2.509. Potentiodynamic polarization (PP) tests were performed with a range of approximately OCP±0.3 V at 0.2 mV/s scan rate. In all cases, five samples of each casting were tested.

3. Results and discussion

3.1. Microstructure

Optical micrographs obtained from samples F, FP and P are presented in Figure 1(a-f). Samples of the non-etched images used for analyzing graphite morphology are shown in Figure 1(a, c, e) while etched samples for analysis of the matrix are presented in Figure 1(b, d, f). A summary of the quantitative metallographic analysis performed on the samples, along with the hardness evaluation (HB) is reported in Table 2.

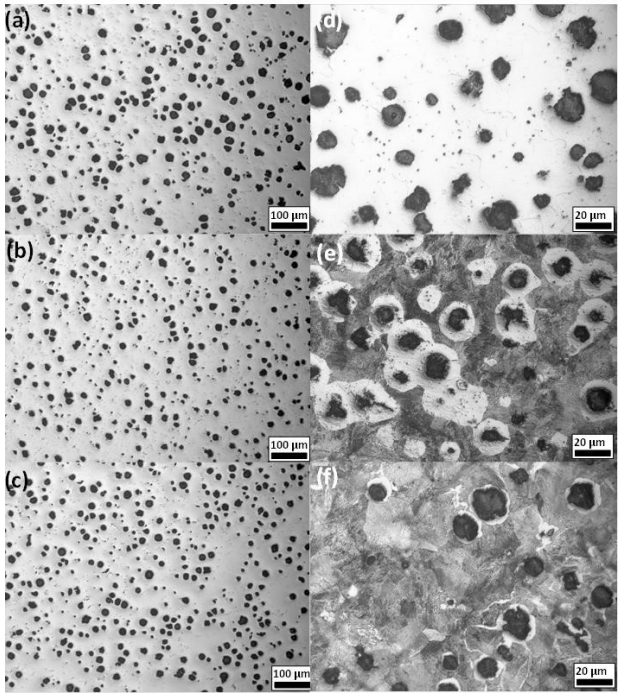

Fig. 1. Microstructure analysis by optical microscopy of samples F (a), (b); FP (c), (d); and P (e), (f). Nital 2% etch employed for images (b), (d) and (f)

Table 2.
Summary of the quantitative metallographic and hardness analysis performed for graphite nodule classification and matrix characterization on samples F (0%Cu-0.09%Mn), FP (0.38%Cu-0.40%Mn) and P (0.69%Cu-0.63%Mn)

SAMPLE	MATRIX	NODULARITY	NODULES	CLASS	HB
F	100% Ferrite	89.0%	198 mm^{-2}	V	140 ± 5
FP	30% Ferrite 70% Pearlite	90.1%	193 mm^{-2}	V	210 ± 9
P	5% Ferrite 95% Pearlite	92.7%	215 mm^{-2}	V	230 ±4

By adopting the chemical composition values chosen presented in Table 1, it was possible to obtain a certain equilibrium in graphite morphology and distribution in the different samples, with exception of casting P which exhibited a slightly higher graphite count (215 nodules per mm^2 compared to 198 and 193 for the F and FP samples, respectively), which accounted for a relatively larger nodularity area (92.7% compared to 89.0% and 90.1% for the F and FP samples, respectively). Despite these differences, according to the ASTM E2567-16a standard, all alloys exhibited class V graphite nodules. As expected, with larger amounts of Cu and Mn it was possible to increase the relative volume fraction of pearlite to 95% (0.69%Cu-0.63%Mn), compared to the fully ferritic matrix observed with no Cu additions and the 30/70 ferrite-pearlite ratio observed for sample FP (with 0.38%Cu-0.40%Mn). Also as expected, the higher pearlite content was also connected to an increase in hardness – a linear relation was identified (with a 0.998 R^2 coefficient), indicating a similar pearlite hardness for samples FP and P (between 235 and 240 HB).

3.2. Corrosion behavior

The corrosion behavior of the F, FP and P ductile irons are investigated in Fig. 2, in which the PP diagram is shown, and Fig. 3(a-b), in which the EIS results are reported according to Nyquist and Bode representations, respectively. The equivalent circuit model used to analyze the EIS data is in turn presented in Figure 4 and a summary of the corrosion parameters obtained by analyzing the experimental results is presented in Table 3.

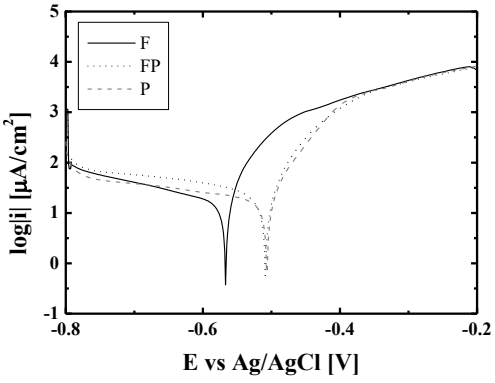

Fig. 2. Potentiodynamic polarization (PP) diagrams obtained for samples F, FP and P in 3.5wt.% NaCl solution

The polarization diagrams presented in Figure 2 highlight on the active corrosion behavior of the analyzed samples. The samples did not exhibit passive behavior in the 3.5wt.%NaCl solution even when polarizing to 1.5V, consistent with previous reports on the corrosion resistance of ductile iron castings [7, 8]. It is possible to notice that samples exhibit similar cathodic and anodic behavior. The anodic Tafel slopes determined for each case remained in the range of 30 to 40 mV/decade, which correspond to the dissolution of Fe in the form of Fe^{2+} by either Bockris or Heusler mechanisms, respectively. In neutral-pH aerated solutions, the expected cathodic reaction is $2H_2O + O_2 + 4e^- \rightarrow 4OH^-$, which corresponds to a theoretical Tafel slope of 29.5 mV/decade. A significant deviation was, however, found in the experimental values (on average close to 300 mV/decade) which can be an indication that the cathodic reaction is partially under diffusion control, *i.e.* as the overvoltage becomes more cathodic the reaction rate increases at a lower rate than expected because the O_2 molecules required for the reaction are slow to diffuse from the electrolyte bulk to the sample surface.

Concerning the results of the EIS measurements presented in Figure 3(a), it is possible to notice that the Nyquist plots reveal the presence of a depressed capacitive arc. Further characteristics of the materials electrochemical impedance behavior are evidenced in Figure 3(b), which indicates that the arc shown in Figure 3(a) has contributions of two time constants (as revealed by the inflection point signaled by the arrow labeled as $R_s + R_{cp}$). Quantitative analysis of the data (Table 3) was performed by using the model presented in Figure 4, which takes into account the presence of an oxide film on the metal surface which is partially permeated by the electrolyte (either by the presence of cracks or pores or simply because of incomplete surface coverage) [13].

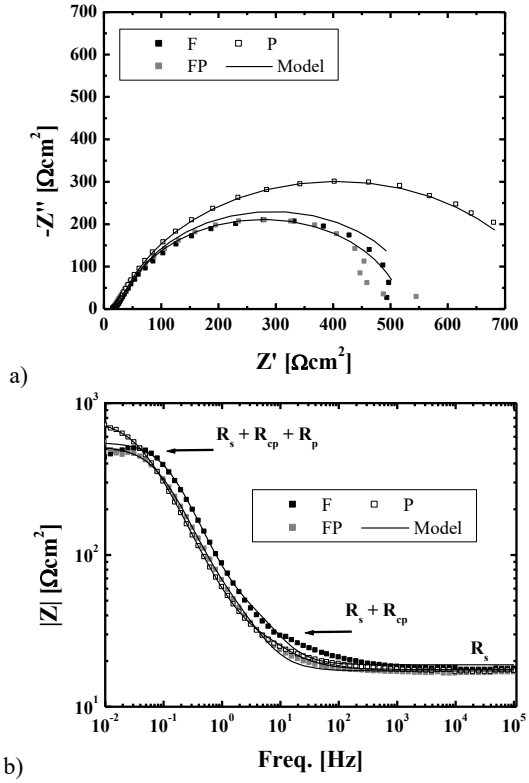

Fig. 3. EIS results obtained for the F, FP and P samples in 3.5wt.% NaCl at the OCP: (a) Nyquist diagram and (b) Bode diagram

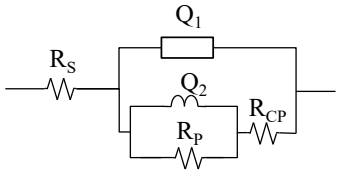

Fig. 4. Equivalent circuit model used for analyzing the EIS data

Thus, two electrochemical interfaces are present in the system: metal/electrolyte (with polarization resistance given by R_p) and the oxide/electrolyte (with polarization resistance given by R_{cp}). The formation of an oxide film can be expected because of the exposure to the 1.5 h exposure to electrolyte, prior to EIS and PP analyses, for OCP stabilization. The whole ensemble is formed still of a third impedance (R_s) due to the solution itself. The overall electrochemical impedance of the system is (R_s + R_{cp} + R_p) appears as the low frequency plateau signaled by the arrow in Figure 3(b). For modelling the non-ideal capacitive arcs, constant phase elements where used (Q_1 and Q_2). It is worth noticing that the solution impedance (R_s) remained practically constant in all tested situations, a positive indication that testing conditions remained consistent among different samples. The R_{cp} values obtained for the F, FP and P irons also remained within the corresponding standard deviation ranges and are indicative that, for all tested materials, the surface oxides do not form a compact layer which could be characterized as a stable passive film.

The results of the PP experiments summarized in Table 3 reveal that a shift of E_{corr} to more positive values with the presence of pearlite in the matrix (and Cu in the alloy composition), indicating less reactive behavior and an increase in corrosion resistance. This trend was not reflected in the corrosion rate, since the i_{corr} values determined by PP for all samples remained within the experimental standard deviations. However, the R_p values determined by EIS – which are expected to be inversely proportional to i_{corr} – also indicated an improvement in corrosion resistance connected to the increase in Cu composition. The values registered in Table 3 are consistent with previous investigations of the electrochemical corrosion behavior of ductile cast irons [7, 14]. For example, Arenas *et al*. [14] also reported a shift in E_{corr} of approximately 50 mV in the positive direction of pearlitic ductile (obtained with the addition of 0.68%Mn and 0.78%Cu) compared to a ferritic casting (0.19%Mn and 0.03%Cu) and values of i_{corr} between 10.3 and 28.3 μA/cm^2 in dilute NaCl solutions.

Table 3.
Summary of the electrochemical corrosion analyses performed by EIS and PP in 3.5wt.% NaCl containing naturally dissolved O_2 (E_{corr} – Corrosion potential; i_{corr} – corrosion current density; R_s – solution resistance; R_{cp} – oxide pore resistance; R_p – polarization resistance)

	E_{CORR} (V)	I_{CORR} (MA/CM^2)	R_S (ΩCM^2)	R_{CP} (ΩCM^2)	R_P (ΩCM^2)
F	-0.56 ± 0.008	25 ± 5.1	23 ± 1.1	55 ± 15.7	630 ± 191
FP	-0.51 ± 0.004	30 ± 8.7	22 ± 0.9	95 ± 34.3	590 ± 163
P	-0.51 ± 0.009	31 ± 1.2	22 ± 0.8	67 ± 22.3	960 ± 76

The addition of Cu has previously found to have a positive influence on corrosion behavior ductile irons in the austempered and as-cast conditions, which was attributed to an observed decrease in graphite nodule count with 1%Cu and consequently a reduced propensity for graphite corrosion [7]. In this work, however, since the graphite nodule count was found in fact to be increased with the amount of Cu, the positive influence in corrosion behavior is supposed to be attributed to other factors. According to Yamamoto *et al* [15], the dissolution rate of ferritic materials is reduced by the presence of Cu due to the formation of surface deposits and a decrease in the effective anodic reaction area by the precipitation of metallic Cu o the alloy surface. In the present study, precipitation can be expected since in both FP and P irons Cu content exceeds the theoretical solubility limit in ferrite (0.2%). These considerations are consistent with the results presented in Table 3, which indicated that increasing the amounts of Cu led to a positive variation in the alloy polarization resistance (R_P), while the impedance due to surface oxide films (R_{cp}) remained unaltered.

4. Conclusions

In the present work, the electrochemical corrosion behavior of ferritic, ferritic-pearlitic and pearlitic ductile cast irons containing, respectively, 0, 0.38 and 0.69%Cu was investigated by potentiodynamic polarization and electrochemical impedance spectroscopy. By using these compositions, it was possible to preserve graphite nodule morphology while modifying the metallic matrix (completely ferritic, partially ferritic-pearlitic and mostly pearlitic for the 0, 0.38 and 0.69%Cu additions, respectively). In addition, it was possible to show that increasing Cu concentration in the cast irons led to higher values of the corrosion potential and polarization resistance – indications of an improvement in corrosion resistance.

Acknowledgements

This work was supported by projects PIBIC PUC Minas (2016-241-S2), FIP PUC Minas (2019/22544-1S) and CNPq (PQ grant 306269/2016-3).

References

[1] Guo, X., Stefanescu, D.M., Chuzhoy, L. & Pershing, M.A. (1997). A mechanical properties model for ductile iron. *Transactions of the American Foundrymen's Society*. 105, 47-54.

[2] Riposan, I., Chisamera, M. & Stan, S. (2010). Performance of heavy ductile iron castings for windmills. *China Foundry*. 7(2), 163-170.

[3] Peng, J.Z., Liu, L.X. & Yang, Z.X. (2010). Quality Control Measures for Heavy Ductile Iron Hub of Wind Turbine Generator. *Foundry*. 59, 969-972.

[4] Al-Hashem, A., Abdullah, A. & Riad W. (2001). Cavitation corrosion of nodular cast iron (NCI) in seawater Microstructural effects. *Materials Characterization*. 47(5), 383-388. DOI: 10.1016/S1044-5803(02)00185-7.

[5] Song, Y., Jiang, G., Chen, Y., Zhao, P. & Tian, Y. (2017). Effects of chloride ions on corrosion of ductile iron and carbon steel in soil environments. *Scientific Reports*. 7, 6865. DOI: 10.1038/s41598-017-07245-1.

[6] Yürektürk, Y. & Baydoğan, M. (2018). Characterization of ferritic ductile iron subjected to successive aluminizing and austempering. *Surface and Coatings Technology*. 347, 142-149. DOI: 10.1016/j.surfcoat.2018.04.083.

[7] Hsu, C.-H. & Chen, M.-Li. (2010). Corrosion behavior of nickel alloyed and austempered ductile irons in 3.5% sodium chloride. *Corrosion Science*. 52(9), 2945-2949. DOI: 10.1016/j.corsci.2010.05.006.

[8] Hsu, C.-H. & Lin, K.-T. (2014). Effects of Copper and Austempering on Corrosion Behavior of Ductile Iron in 3.5 Pct Sodium Chloride. *Metallurgical and Materials Transactions A*. 45(3), 1517-1523. DOI: 10.1007/s11661-013-2059-2.

[9] Han, Ch.F., Wang, Q.Q., Sun, Y.F. & Li, J. (2015). Effects of Molybdenum on the Wear Resistance and Corrosion Resistance of Carbidic Austempered Ductile Iron. *Metallography, Microstructure, and Analysis*. 4(4) 298-304. DOI: 10.1007/s13632-015-0215-3.

[10] Medyński, D. & Janus, A. (2016). Effect of Chemical Composition on Structure and Corrosion Resistance of Ni-Mn-Cu Cast Iron. *Archives of Foundry Engineering*. 16(3), 59-62. DOI: 10.1515/afe-2016-0050.

[11] Ige, O.O,. Olawale, O.J., Oluwasegun, K.M., Aribo, S., Obadele, B.A. & Olubambi, P.A. (2017). *Procedia Engineering*. 7, 579-583. DOI: 10.1016/j.promfg.2016.12.084.

[12] Boudot, A., Gerval, V., Oquab, D., Lacaze, J. & Santos, H. (1997). The role of manganese and copper in the eutectoid transformation of spheroidal graphite cast iron. *Metallurgical and Materials Transactions A*. 28(10), 2015-2025. DOI: 10.1007/s11661-997-0158-7.

[13] Sancy, M., Gourbeyre, Y., Sutter, E.M.M. & Tribollet, B. (2010). Mechanism of corrosion of cast iron covered by aged corrosion products: Application of electrochemical impedance spectrometry. *Corrosion Science*. 52(4), 1222-1227. DOI: 10.1016/j.corsci.2009.12.026.

[14] Arenas, M.A., Niklas, A., Conde, A., Méndez, S., Sertucha, J. & Damboronea, J.J. (2014). Comportamiento frente a la corrosión de fundiciones con grafito laminar y esferoidal parcialmente modificadas con silicio en NaCl 0,03 M. *Revista de Metalurgia*. 50(4), e032. DOI: 10.3989/revmetalm.032.

[15] Yamamoto, A. Ashiura, T. & Kamisaka, E. (1986). Mechanism of improvement on corrosion resistance by copper addition to ferritic stainless steels. *Corrosion Engineering*. 35(8), 448-454.